

## Dof splitting $p$ -adaptive meshless method

Myung-Seok Kang<sup>†</sup> and Sung-Kie Youn<sup>‡</sup>

Department of Mechanical Engineering, KAIST, Taejeon 305-701, Korea

**Abstract.** A new  $p$ -adaptive analysis scheme for  $hp$ -clouds method is presented. In the scheme, refined global equations are resolved into two parts, one of them being related to the newly appended dof's. The solution obtained in previous analysis step is reflected in the force vector. The size of the  $p$ -adaptive equation consisting of the newly appended dof's is much smaller than the original equation. Consequently, the computational cost is drastically decreased. Through numerical examples, the efficiency and efficacy of the method in comparison with the existing  $p$ -refinement scheme of the  $hp$ -clouds have been demonstrated.

**Key words:** meshless method; meshfree method;  $hp$ -clouds method;  $p$ -refinement; dof splitting;  $p$ -adaptive meshless method; DSPMM.

---

### 1. Introduction

The motivation behind meshless methods is to avoid the effort generating mesh in finite element method (FEM). The concept of analysis without mesh is realized first in the methods of smoothed particle hydrodynamics (SPH) (1997) and particle-in-cell method (PIC) (Harlow 1964). These methods are basically particle methods which treat a body as a set of particles.

In 1992, Nayroles *et al.* (1992) proposed a meshless method named as diffuse element method (DEM) which is based on moving least square approximation. Belytschko *et al.* (1994) developed an element-free Galerkin method (EFGM) which improves the accuracy of the DEM by using the exact derivative of shape function and introducing Lagrange multipliers to exactly satisfy essential boundary conditions. They showed the fact that a meshless method could be effectively applied to the crack propagation problem and  $p$ -refinement could be achieved by introducing singular functions to basis function to reproduce the singularity near crack tip. This scheme does not require increased number of fundamental variables but one should know the characteristics of the solution before the analysis. The posteriori error estimator is also developed. The error criterion detects the difference between the stresses obtained by the direct derivatives of displacements and the projected stresses. The projected stresses are obtained by the linear combination of the shape functions and nodal stresses.

Liu *et al.* (1997) presented a reproducing kernel particle method (RKPM) based on the SPH method. The SPH method does not satisfy completeness conditions. They recognized that the inaccuracy of the SPH method near the boundary of the domain is due to the lack of completeness of the approximation, and introduced correction terms to satisfy the completeness. In RKPM, the

---

<sup>†</sup> Graduate Student

<sup>‡</sup> Professor

error estimator is based on the multi-resolution analysis in which the solution is resolved into two parts-one with lower frequency components and the other with higher frequency components. The error estimator judges that the error resides in the region where the effect of the high frequency components is dominant. The resulting shape function of RKPM is the practically the same with that of EFGM even though the formulation is driven in different way.

Duarte *et al.* (1997) devised the *hp*-clouds method that facilitates *p*-refinement in the organized manner. The higher order *hp*-clouds shape functions are easily generated by the multiplication of the partition of unity functions and basis functions. The completeness of the approximation can be increased without the increase of the radius of influence.

In this paper, a dof splitting *p*-adaptive meshless method (DSPMM) is presented. In *p*-refinement of *hp*-clouds method additional dof's are appended to the nodes to which refinements are enforced. As a result, new shape functions are appended which do not influence the previously introduced shape functions. The algebraic equations constructed with existing dof's and newly appended dof's are not completely different from the equation of previous analysis. Furthermore the error of the solution is concentrated in local region in most problems, and the *p*-refined dof's are appended to the nodes in the region when the solution is not accurate enough. In DSPMM, the values of the existing dof's are preserved in the *p*-refined algebraic equations thus the resulting equations are solved for only newly appended dof's. Consequently the computational cost is considerably decreased.

## 2. Meshless approximation

### 2.1 EFG approximation

The EFG method constructs meshless shape functions for arbitrarily distributed nodes without nodal connectivity, and the shape functions are complete up to the given order. The derivation of the EFG shape functions is based on the moving least square method in which the local approximation  $u^h(\mathbf{x})$  of the function  $u(\mathbf{x})$  is

$$u^h(\mathbf{x}) = \sum_{i=1}^m p_i(\mathbf{x}) a_i(\mathbf{x}) \quad (1)$$

where  $m$  is the number of terms in the basis,  $p_i(\mathbf{x})$  monomial basis functions, and  $a_i(\mathbf{x})$  their coefficients. Using the moving least square method the coefficients  $a_i(\mathbf{x})$  are determined by minimizing the following sum of weighted squares of the differences between the nodal values and their local approximation with respect to the coefficients  $a_i(\mathbf{x})$ .

$$J = \sum_I^{N_p} w(\mathbf{x} - \mathbf{x}_I) [u(\mathbf{x} - \mathbf{x}_I) - u(\mathbf{x})]^2 \quad (2)$$

In the above,  $N_p$  is the number of nodes and  $w(\mathbf{x} - \mathbf{x}_I)$  is a weight function with compact support. The coefficient  $a_i(\mathbf{x})$  is obtained as follows:

$$\mathbf{a}(\mathbf{x}) = \mathbf{A}(\mathbf{x})^{-1} \mathbf{B}(\mathbf{x}) \mathbf{u} \quad (3)$$

where

$$A_{ij}(\mathbf{x}) = \sum_{l=1}^{Np} w(\mathbf{x} - \mathbf{x}_l) p_i(\mathbf{x}_l) p_j(\mathbf{x}_l) \quad (4)$$

$$B_{il}(\mathbf{x}) = w(\mathbf{x} - \mathbf{x}_l) p_i(\mathbf{x}_l). \quad (5)$$

Substituting the coefficient  $a_i(\mathbf{x})$  in Eq. (3) into Eq. (1), following is obtained.

$$u(\mathbf{x}) = \sum_{l=1}^{Np} \varphi_l(\mathbf{x}) u_l \quad (6)$$

where  $\varphi_l(\mathbf{x})$  given by

$$\varphi_l(\mathbf{x}) = \sum_{i=1}^m p_i(\mathbf{x}) [A(\mathbf{x})^{-1} B(\mathbf{x})]_{il} \quad (7)$$

### 2.1 *H*-*p* clouds approximation

*H**p*-clouds method provides higher order basis functions of approximation with very low computational cost. The higher order basis functions are generated by the multiplication of the partition of unity functions and the monomial basis. When the partition of unity function  $S_{Np}^k(\mathbf{x}) = \{\varphi_\alpha^k(\mathbf{x})\}_{\alpha=1}^{Np}$  is complete up to the order  $k$  and the monomial basis function  $L_{ijl}(x, y, z)$  is complete up to the order  $p$ . The family of *hp*-clouds shape function in  $R^3$  is expressed as follows:

$$F_N^{k,p} = \{ \{ \varphi_\alpha^k(\mathbf{x}) \} \cup \{ \varphi_\alpha^k(\mathbf{x}) L_{ijl}(\mathbf{x}) \}; 1 \leq \alpha \leq N; 0 \leq i, j, l \leq p, i \text{ or } j \text{ or } l > k; p \geq k \} \quad (8)$$

where

$$L_{ijl}(x, y, z) = L_i(x) L_j(y) L_l(z) \quad 0 \leq i, j, l \leq p \quad (9)$$

In the above,  $L_i(x)$ ,  $L_j(y)$  and  $L_l(z)$  is monomials of  $x$ ,  $y$  and  $z$ , respectively. Then, the *hp*-clouds shape function  $\varphi_\alpha^{k,p} \in F_N^{k,p}$  is complete up to the order  $p$  and the typical *hp*-clouds approximation is

$$u^h(\mathbf{x}) = \sum_{l=1}^{Np} \varphi_l^k(\mathbf{x}) \left[ u_l + \sum_i^{n_l} b_{il} q_i(\mathbf{x}) \right] \quad (10)$$

Here  $q_i(\mathbf{x})$  is a monomial basis generated by the Eq. (9) and the order can be greater than  $k$  since the partition of unity  $S_{Np}^k(\mathbf{x})$  is complete up to the order  $k$ .

### 2.2 Treatment of essential boundary conditions

The general EFG approximation does not satisfy the Kronecker delta condition  $\varphi_l(\mathbf{x}_j) \neq \delta_{lj}$  at all the nodes. Consequently, the shape functions are not interpolants. Thus the property makes the imposition of essential boundary conditions cumbersome.

Several methods to impose essential boundary conditions have been developed by different researchers. Among them are the introduction of Lagrange multipliers (Belytschko *et al.* 1994), the formulation using the modified variational principle (Lu *et al.* 1994), and coupling the meshless shape functions with those of FEM (Krongauz and Belytschko 1996), etc. They lack computational efficiencies or traits of meshless methods.

In Kang and Youn (2001), admissible EFG shape functions are developed. The kinematically admissible EFG shape functions are derived by the modification of weight functions using auxiliary weight functions. The shape functions satisfy Kronecker delta condition on the boundary nodes where essential boundary conditions are specified and the interpolation property is kept intact along the boundary lines.

An auxiliary weight function is defined to have an origin at a boundary node or the boundary segment where essential boundary condition is prescribed. The value of the auxiliary weight function is zero at the origin and monotonically increases up to 1. Then the weight functions are modified as the following equation.

$$\bar{w}_I(\mathbf{x}) = w_I(\mathbf{x}) \prod_{\substack{1 \leq J \leq N_{\text{essBc}} \\ I \neq J}} f_{IJ}(\mathbf{x}) \quad (11)$$

where,  $N_{\text{essbc}}$  is the number of nodes or boundary segments on which essential boundary conditions are specified. The function  $f_{IJ}(\mathbf{x})$  is the auxiliary function defined between the node  $I$  and the index  $J$ . The subscript  $I$  denotes the node where the weight function is defined and the subscript  $J$  denotes the  $J$ th essential boundary condition to be imposed. In the case where essential boundary condition is imposed on a node, let the node number at which essential boundary  $J$  is imposed be  $J$  for convenience.

The essential boundary condition  $J$  could be specified on the boundary segment consisting of two nodes  $J_1$  and  $J_2$ . The boundary segment is, in general, a curved line in two dimensional space.

The auxiliary weight function is defined as a function of a normalized distance  $\rho_{IJ}$ ,

$$\rho_{IJ} = \frac{d_J[\mathbf{x}]}{d_J[\mathbf{x}_I]} \quad (12)$$

where  $d_J[\mathbf{x}]$  is a distance between the evaluation point  $\mathbf{x}$  and the boundary  $J$  where essential boundary conditions are prescribed.

The definition of the distance  $d_J[\mathbf{x}]$  is clear by itself when essential boundary condition is prescribed on a node.

$$d_J[\mathbf{x}] = \|\mathbf{x} - \mathbf{x}_J^{bc}\| \quad (13)$$

In the above,  $\mathbf{x}$  is an evaluation point, and  $\mathbf{x}_J^{bc}$  is the position of  $J$ th restrained node. When the essential boundary conditions are prescribed on a boundary segment with two end nodes  $J_1$  and  $J_2$ , the distance is defined as a minimum distance from the evaluation point to the boundary segment.

$$d_J[\mathbf{x}] = \begin{cases} d_{J_1}[\mathbf{x}] = \|\mathbf{x} - \mathbf{x}_{J_1}\|, & \text{if } x \text{ is in the region A} \\ \|\mathbf{x} - \mathbf{x}_J\|, & \text{if } x \text{ is in the region B} \\ d_{J_2}[\mathbf{x}] = \|\mathbf{x} - \mathbf{x}_{J_2}\|, & \text{if } x \text{ is in the region C} \end{cases} \quad (14)$$

where, the region A, B and C are shown in Fig. 1.

The EFG shape function with modified weight function by the auxiliary weight function is sufficiently smooth and satisfy the Kronecker delta condition. However Eq. (7) for the shape function is not valid on the boundary where essential boundary conditions are prescribed. The matrix  $A(\mathbf{x})$  is singular since the auxiliary function has the value of zero on the boundary.

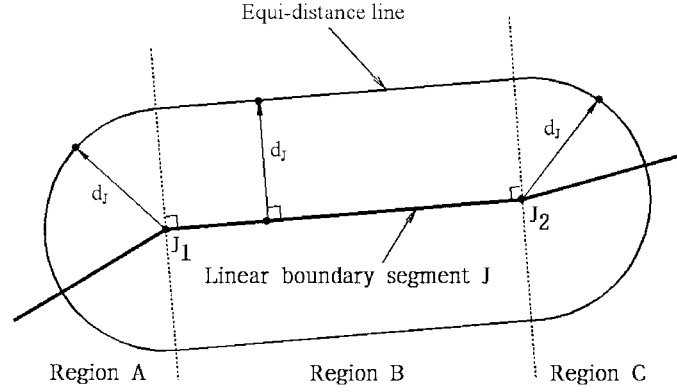


Fig. 1 Distance  $d_j[x]$  between a point  $x_i$  and boundary segment  $J$

Examples of the auxiliary weight functions are

$$f_{IJ}(\mathbf{x}) = \hat{f}(\rho_{IJ}) = \begin{cases} 1 - (1 - \rho_{IJ})^2, & \text{if } 0 \leq \rho_{IJ} < 1 \\ 1, & \text{if } \rho_{IJ} \geq 1 \end{cases} \quad \text{for } C^1 \text{ continuity} \quad (15)$$

$$f_{IJ}(\mathbf{x}) = \hat{f}(\rho_{IJ}) = \begin{cases} 1 - (1 - \rho_{IJ})^3, & \text{if } 0 \leq \rho_{IJ} < 1 \\ 1, & \text{if } \rho_{IJ} \geq 1 \end{cases} \quad \text{for } C^2 \text{ continuity} \quad (16)$$

### 3. Variational formulation for dof splitting $p$ -adaptive meshless method

We consider the linear elastic problem defined on the domain  $\Omega$  bounded by boundary  $\Gamma$ . The equilibrium equation is

$$\nabla \cdot \boldsymbol{\sigma} + \mathbf{b} = \mathbf{0} \quad \text{in } \Omega \quad (17)$$

where  $\boldsymbol{\sigma}$  is the stress tensor and  $\mathbf{b}$  a body force vector. The traction boundary condition and the displacement boundary condition are respectively given as follows:

$$\boldsymbol{\sigma} \cdot \mathbf{n} = \bar{\mathbf{t}} \quad \text{on } \Gamma_t \quad (18a)$$

$$\mathbf{u} = \bar{\mathbf{u}} \quad \text{on } \Gamma_u \quad (18b)$$

where the bar denotes the prescribed boundary values, and  $\mathbf{n}$  the unit normal vector to the boundary  $\Gamma_t$ .

Consider the trial function space  $U$  and the test function space  $V$ .

$$U = \{ u \in H^1(\Omega), u = \bar{u} \quad \text{on } \Gamma_u \} \quad (19)$$

$$V = \{ v \in H^1(\Omega), v = 0 \quad \text{on } \Gamma_u \} \quad (20)$$

Now, the variational form of the equilibrium Eq. (17) becomes

$$\int_{\Omega} \delta(\nabla_s v^T) : \boldsymbol{\sigma} d\Omega - \int_{\Gamma_t} \delta v^T \cdot \mathbf{b} d\Gamma - \int_{\Gamma_u} \delta v^T \cdot \bar{\mathbf{t}} d\Gamma = 0, \quad \forall \delta v \in H^1 \quad (21)$$

where  $\nabla_{,s}v^T$  is the symmetric part of  $\nabla v^T$ .

The discrete equation is obtained by the introduction of the  $hp$ -cloud shape functions  $\phi^o(x)$ . The superscript  $o$  indicates that the corresponding term is related to the analysis of unrefined problem.

$$K^{oo}\bar{u}^o = F^o \quad (22)$$

where

$$K_{IJ}^{oo} = \int_{\Omega} B_I^{oT} D B_J^o d\Omega \quad (23a)$$

$$F_I^o = \int_{\Gamma_i} \phi_I^o \bar{t} d\Gamma + \int_{\Omega} \phi_I^o b d\Omega \quad (23b)$$

Once the result of analysis is obtained the region to be refined is determined by the posteriori error estimator (Chung *et al.* 1998). A  $p$ -refinement process is achieved by appending additional dof's to the appropriate nodes in  $hp$ -clouds method. We can write the  $p$ -refined solution  $u^p(x)$  as the sum of the solution of unrefined problem  $u^o(x)$  and the correction  $u^r(x)$  obtained by the adaptive analysis. The trial function  $u^p(x)$  and the test function  $\delta v^p(x)$  are expressed as follows:

$$\delta v^p(x) = \delta v^o(x) + \delta v^r(x) \quad (24)$$

$$u^p(x) = u^o(x) + u^r(x) \quad (25)$$

Note that the solution of unrefined problem  $u^o(x)$  is in the space  $U$ , but the correction of the solution  $u^r(x)$  should be in the space  $V$  since all the essential boundary conditions are already satisfied by the solution  $u^o(x)$ . This is easily achieved by using the modified EFG shape functions with the auxiliary weight function mentioned in Section 2.2.

The variational formulation for the  $p$ -refined problem using the expressions of the Eq. (24) and Eq. (25) is

$$\begin{aligned} \delta \Pi = \int_{\Omega} \nabla_{,s}(v^o + v^r)^T : (\sigma^o + \sigma^r) d\Omega - \int_{\Gamma_i} \delta(v^o + v^r)^T : \bar{t} d\Gamma - \int_{\Omega} \delta(v^o + v^r)^T : b d\Omega \\ \forall u^o \in U, \forall u^r \in V, \forall v^o \in V, \forall v^r \in V \end{aligned} \quad (26)$$

The matrix form of the discretized  $p$ -refined equations is

$$\begin{bmatrix} K^{oo} & K^{or} \\ K^{ro} & K^{rr} \end{bmatrix} \begin{pmatrix} u^o \\ u^r \end{pmatrix} = \begin{pmatrix} F^o \\ F^r \end{pmatrix} \quad (27)$$

where

$$K_{IJ}^{oo} = \int_{\Omega} B_I^{oT} D B_J^o d\Omega, \quad (28a)$$

$$K_{IJ}^{or} = \int_{\Omega} B_I^{oT} D B_J^r d\Omega, \quad (28b)$$

$$K_{IJ}^{ro} = \int_{\Omega} B_I^{rT} D B_J^o d\Omega, \quad (28c)$$

$$K_{IJ}^{rr} = \int_{\Omega} B_I^{rT} D B_J^r d\Omega, \quad (28d)$$

$$F_I^o = \int_{\Gamma_i} \phi_I^o \bar{t} d\Gamma + \int_{\Omega} \phi_I^o b d\Omega, \quad (28e)$$

$$F_I^r = \int_{\Gamma_I} \phi_I^r \bar{t} d\Gamma + \int_{\Omega} \phi_I^r b d\Omega, \quad (28f)$$

Now, we can write the  $p$ -refined equation Eq. (27) as the two coupled equations.

$$K^{oo} u^o = F^o - K^{or} u^r \quad (29)$$

$$K^{rr} u^r = F^r - K^{ro} u^o. \quad (30)$$

In many problems, the errors are localized in some critical regions. The refinement process is achieved in the region and the solutions are improved by the appended nodes or appended dof's. Considering the  $p$ -adaptive refinement in  $hp$ -clouds method, newly appended higher order shape functions do not affect existing lower order shape functions. Therefore the stiffness matrix  $K^{oo}$  in Eq. (22) is the same as that in Eq. (27). Therefore the Eq. (29) is different in the coupling term  $K^{or} u^r$  from Eq. (22). Assuming that the effect of the coupling term is minor, we can substitute the solution  $u^o$  in Eq. (22) to that in Eq. (30).

In the point of view of the multi-resolutional analysis in RKPM, the error reside in the high frequency part of the approximation solution. Thus the effect of  $p$ -refinement is reflected dominantly in the values of newly appended dof's. In this reason  $u^o$  is not newly calculated from Eq. (29). Only Eq. (30) is used to obtain refined solution. This includes the construction of stiffness matrix  $K^{rr}$  and  $K^{ro}$ , and therefore the computational time to form equations is comparable to that consumed in constructing Eq. (27). However the time required for solving the equations is considerably decreased. When  $N$  is the number of dof's in the problem, the time needed to form the equations is increased in the order of  $N^2$ . On the other hand, the time needed in solving the equations is increased in the order of  $N^3$ . Therefore as the problem size grows, the computational cost of the present scheme will be remarkably decreased.

#### 4. Numerical examples

The efficiency of the dof splitting  $p$ -adaptive meshless method is demonstrated in the following two examples.

When the order of the  $hp$ -cloud shape functions is increased, the order of integration should be also increased because the size of the integration cell is fixed in these examples. The integration cell is, in the examples, a quadrilateral with four nodes. The following order of integration is used.

$$n = 4 \cdot \sqrt{M} \quad (31)$$

where

$n$ =the order of integration

$M$ =maximum order of the shape functions of the nodes at the vertices of a integration cell.

To quantify the numerical accuracy of the two methods the energy error norm is defined as follows:

$$\|E^e\|_2 = \left[ \frac{1}{2} \int_{\Omega} (\boldsymbol{\varepsilon}^h - \boldsymbol{\varepsilon}^{\text{exact}})^T (\boldsymbol{\sigma}^h - \boldsymbol{\sigma}^{\text{exact}}) d\Omega \right]^{\frac{1}{2}} \quad (32)$$

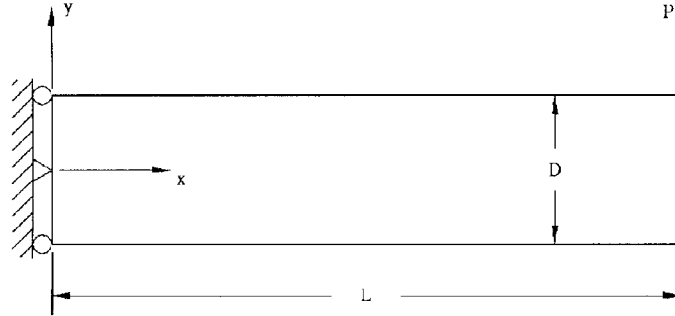


Fig. 2 Cantilever beam

#### 4.1 Cantilever beam

The bending of cantilever beam in Fig. 2 is examined. The beam has a unit width and loaded by a force  $P$  at the end. The analytic solution of the problem is provided by Timoshenko and Goodier (1970) for plane stress case. These are shown in Eqs. (33)-(37)

$$u_x = \frac{Py}{6EI} \left[ (6L - 3x)x + (2 + \nu) \left( y^2 - \frac{D^2}{4} \right) \right] \quad (33)$$

$$u_y = -\frac{P}{6EI} \left[ 3\nu y^2(L - x) + (4 + 5\nu) \frac{D^2 x}{4} + (3L - x)x^2 \right] \quad (34)$$

$$\sigma_{xx} = \frac{P}{I}(L - x)y \quad (35)$$

$$\sigma_{xy} = -\frac{P}{2I} \left( \frac{D^2}{4} - y^2 \right) \quad (36)$$

$$\sigma_{yy} = 0 \quad (37)$$

In numerical model, the displacement distribution in Eqs. (33) and (34) is applied as essential boundary condition along the line  $x=0$  and the load  $P$  is replaced by the traction of Eqs. (35), (36) and (37) along the line  $x=L$ .

Young's modulus  $E=1000$ , Poisson's ratio  $\nu=0.3$  and geometric parameters of  $L=20$ ,  $D=6$  are used. Nodes are uniformly distributed with nodal distance  $h$  and the radii of supports of the shape functions for each node are set to  $2.1h$ .

Fig. 3 shows the nodal distribution and shape functions defined on the nodes of the numerical model with 147 nodes. The dots denote nodes and long vertical bar contacting with a node denotes the corresponding shape function which is used in unrefined analysis. The number of dof's doubles the number of the bars. The other short bars in Figs. 3(b), (c) and (d) denote the appended shape functions. In general  $hp$ -clouds method, all the dof's are solved in each adaptive analysis. However in DSPMM only the appended dof's are solved in adaptive analysis.

Fig. 4 shows the computational costs required in forming and solving equations. As shown in the figure, the computational cost consumed in forming DSPMM equations is almost same as that of  $hp$ -clouds method. However, in the case of DSPMM the computational cost required in solving

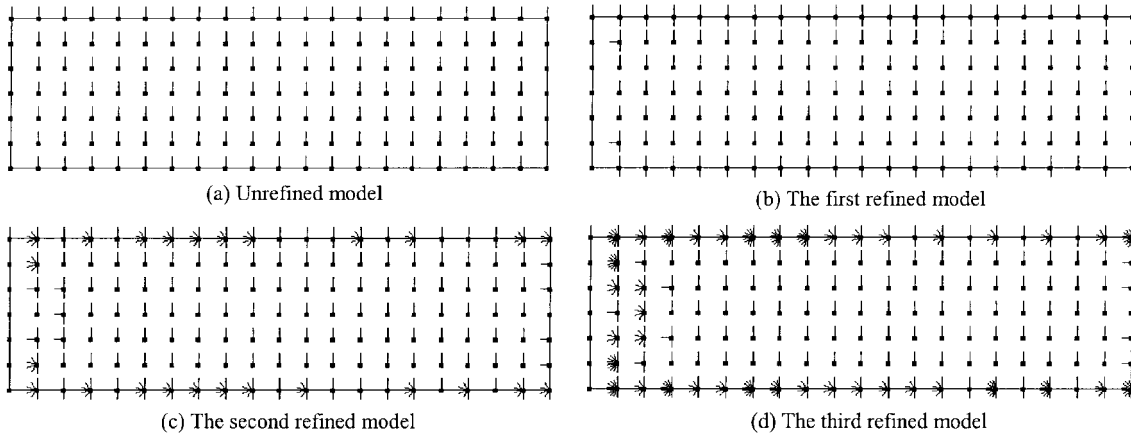


Fig. 3 The numerical model with 147 nodes of the bending of a beam

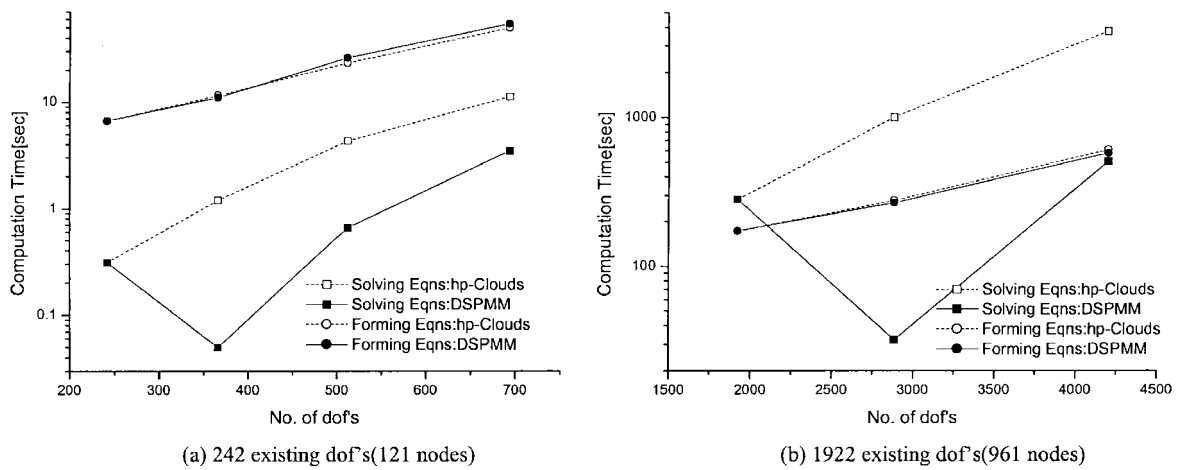


Fig. 4 The computation times required in constructing equations and solving the equation

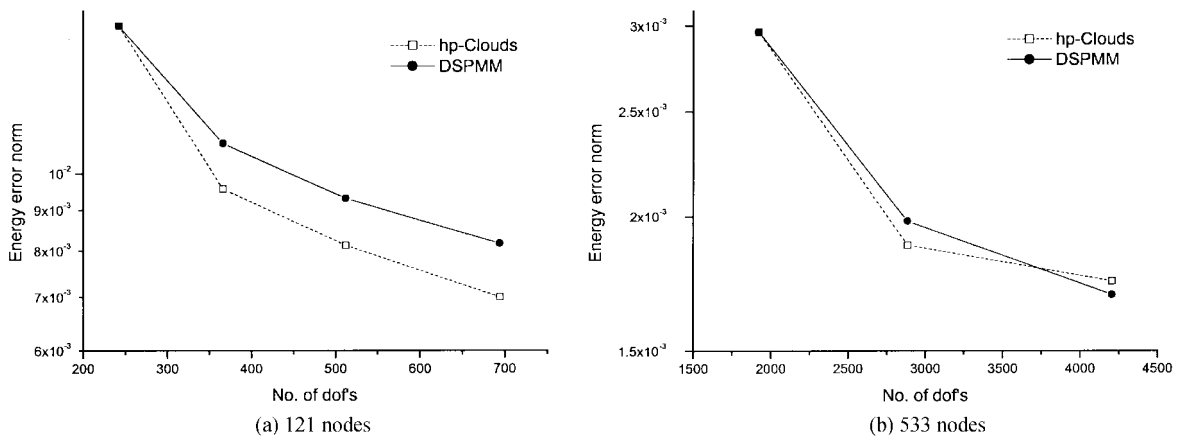


Fig. 5 *P*-convergence for bending of a beam problem

equations is far less than that of *hp*-clouds method.

Fig. 5 shows the accuracies of the *hp*-clouds method and DSPMM. The accuracy of DSPMM is comparable to that of *hp*-clouds method.

#### 4.2 A plate with a hole

The finite quarter plate in Fig. 6 is loaded with the stresses in Eqs. (38), (39) and (40) to reproduce the behavior of the infinite plate with a hole at the origin under uniform unilateral tension  $\sigma$ . The analytical solution of the stress distribution is given by Timoshenko and Goodier (1970) for plane stress case.

$$\sigma_{xx}(x,y) = \sigma \left\{ 1 - \frac{d^2}{r^2} \left( \frac{1}{2} \cos 2\theta + \cos 4\theta \right) + \frac{3d^4}{2r^4} \cos 4\theta \right\} \quad (38)$$

$$\sigma_{yy}(x,y) = \sigma \left\{ -\frac{d^2}{r^2} \left( \frac{1}{2} \cos 2\theta - \cos 4\theta \right) - \frac{3d^4}{2r^4} \cos 4\theta \right\} \quad (39)$$

$$\sigma_{xy}(x,y) = \sigma \left\{ -\frac{d^2}{r^2} \left( \frac{1}{2} \sin 2\theta + \sin 4\theta \right) + \frac{3d^4}{2r^4} \sin 4\theta \right\} \quad (40)$$

where  $(r, \theta)$  are polar coordinates with an origin at the center of the hole. The parameters of the problem used are the width and height  $L=5$ , the radius of the plate  $h=1$ , the uniform lateral tension  $\delta=10$ , Young's modulus  $E=1000$ , and Poisson's ratio  $\nu=0.3$ .

The numbers of nodes used are 121 and 961. The dof's are added by introducing the higher order *hp*-clouds shape functions to the nodes and the refined system is solved by the two different formulation of normal *hp*-clouds method and DSPMM.

Fig. 7 shows the distribution of nodes and shape functions defined on the nodes.

Fig. 8 shows the computational costs required for constructing equations and solving the equations.

The accuracies of *hp*-clouds method and DSPMM are plotted in Fig. 9.

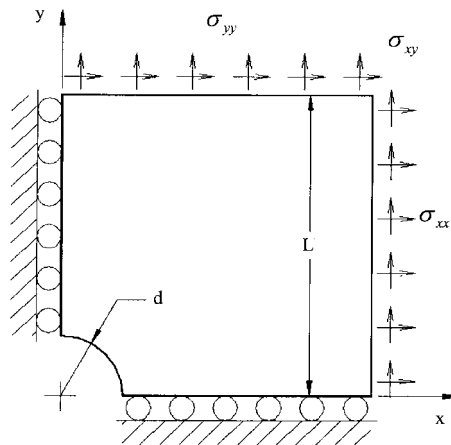


Fig. 6 The finite quarter plate with a central circular hole

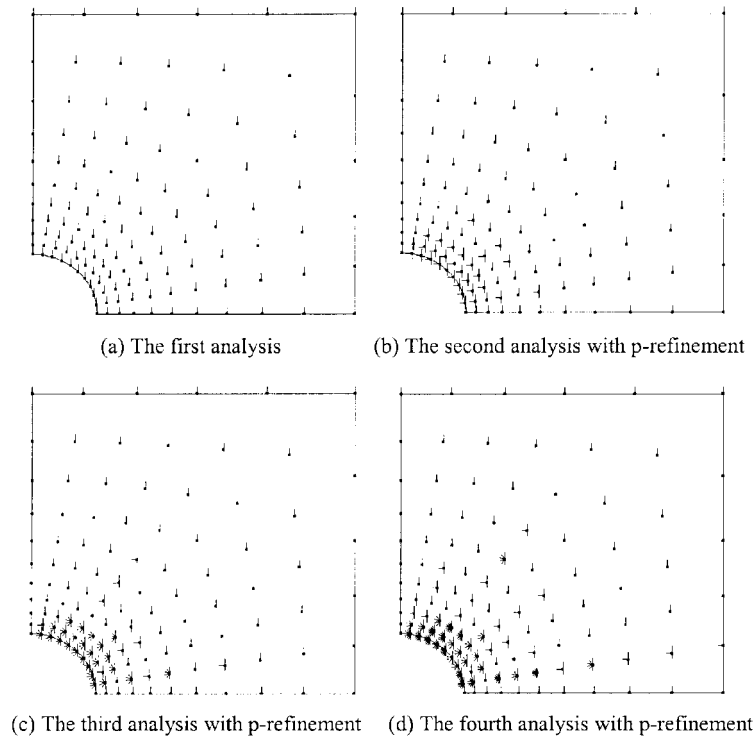


Fig. 7 The shape functions corresponding to each node

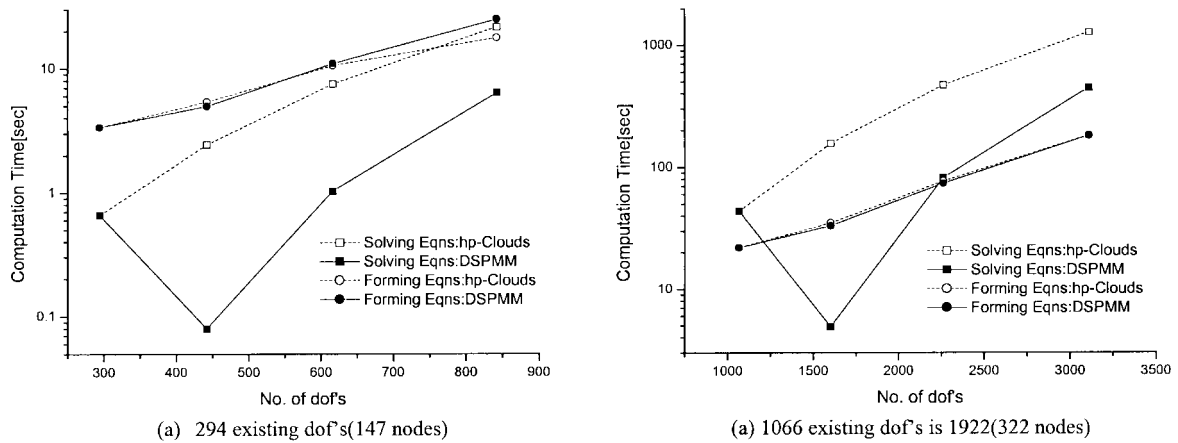


Fig. 8 The computation times required in constructing equations and solving the equation

Comparing the results of the  $p$ -adaptive refinement using  $hp$ -clouds method and DSPMM, the accuracy of the  $hp$ -clouds method turns out to be slightly better than that of the DSPMM. However, in the view of computational costs, the DSPMM is far more efficient than the existing  $p$ -adaptive scheme as the number of dof's is increased.

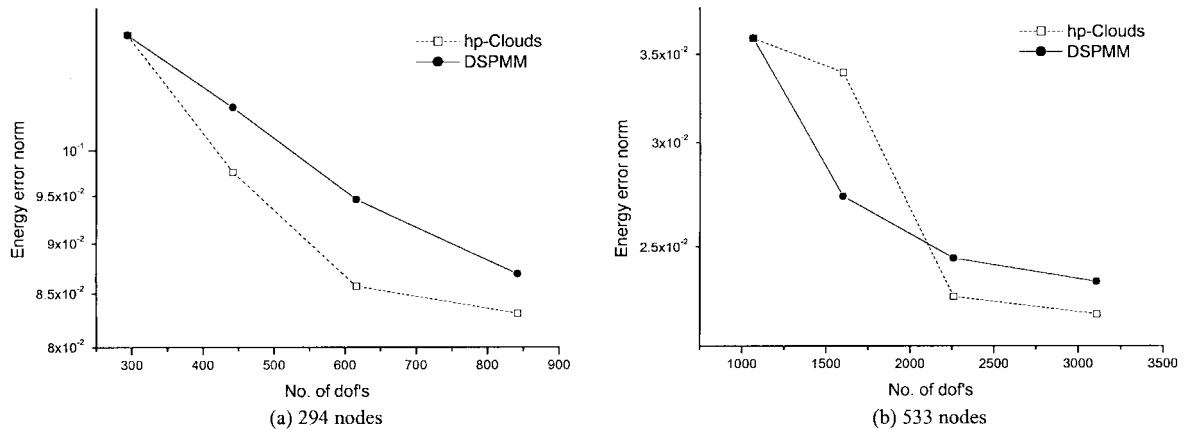


Fig. 9  $P$ -convergence for infinite plate with a hole

## 5. Conclusions

A dof splitting  $p$ -adaptive meshless method (DSPMM) is presented. In this method, only the newly appended dof's are solved in the  $p$ -adaptive analysis. The accuracy and the computational cost requiring to construct the equations are comparable to those of general  $p$ -adaptive  $hp$ -clouds method. However, it needs drastically reduced computational cost in solving the equation. This is a noticeable feature in meshless method since meshless methods normally require very high computational costs when compared with existing numerical method like FEM.

## References

- Belytschko, T., LU, Y.Y., and Gu, L. (1994), "Element-free Galerkin methods", *Int. J. Numer. Meth. Eng.*, **37**, 229-256.
- Chung, H.-J., and Belytschko, T. (1998), "An error estimate in the EFG method", *Computational Mechanics*, **21**, 91-100.
- Duarte, C.A.M., and Oden, J.T. (1995), "Hp clouds - A meshless method to solve boundary-value problems", Technical Rep. 95-05, TICAM, The University of Texas at Austin.
- Harlow, F.H. (1964), "The particle-in-cell computing method for fluid dynamics", *Methods for Computational Physics*, **3**, 319-343.
- Kang, M.-S., and Youn, S.-K. (2001), "Kinematically admissible meshless approximation using modified weight function", *Int. J. Numer. Meth. Eng.*, **50**, 1993-2006.
- Krongauz, Y., and Belytschko, T. (1996), "Enforcement of essential boundary conditions in meshless approximations using finite elements", *Comput. Meth. in Appl. Mech. and Eng.*, **131**, 133-145.
- Liu, W.K., Hao, W., Chen, Y., and Jun, S. (1997), "Multiresolution reproducing kernel particle methods", *Computational Mechanics*, **20**, 295-309.
- Lu, Y.Y., Belytschko, T., and Gu, L. (1994), "A new implementation of the element free Galerkin method", *Comput. Meth. in Appl. Mech. and Eng.*, **113**, 394-414.
- Lucy, L.B. (1997), "A numerical approach to the testing of the fission hypothesis", *The Astronomical J.*, **82**(12), 1013-1024.
- Nayroles, B., Touzot, G., and Villon, P. (1992), "Generalizing the finite element method: diffuse approximation and diffuse elements", *Computational Mechanics*, **10**, 307-318.
- Timoshenko, S.P., and Goodier, J.N. (1970), *Theory of Elasticity*, 3rd edn., McGraw Hill, New York.